S. Afr. J. Chem., 2024, 78, 178–191
https://journals.co.za/content/journal/chem/

Synthesis and characterization of magnetic chitosan-polypyrrole composite for adsorption of tetracyclines from contaminated water

Mpho C. Lefatle[1,2], Lawrence M. Madikizela[3], Vusumzi E. Pakade[4], Philiswa N. Nomngongo[1,2*]

[1]*Department of Chemical Sciences, University of Johannesburg, Doornfontein, South Africa*
[2]*Department of Science and Innovation-National Research Foundation South Africa Research Chair Initiative (DSI-NRF SARChI) in Nanotechnology for Water, University of Johannesburg, Doornfontein, South Africa*
[3]*Institute for Nanotechnology and Water Sustainability, College of Science, Engineering and Technology, University of South Africa, Roodepoort, South Africa*
[4]*Department of Chemistry, College of Science, Engineering and Technology, University of South Africa, Roodepoort, South Africa*

ABSTRACT

The extensive consumption of tetracyclines (TCs) has gained attention due to their toxic effect. The current study reports the synthesis and characterization of magnetic chitosan-polypyrrole (Cs-PPy-Fe_3O_4) composite, which was then used for the adsorption of TCs from aqueous solutions. The synthesized adsorbent had a surface area, pore volume, and pore size diameter of 129 m^2 g^{-1}, 0.32 cm^3 $g^{-1,}$ and 9.9 nm, respectively. Furthermore, the adsorbent had an elemental composition of C (53.6%), O (18.0%), N (12.4%), Fe (12.4%) and O (18.0%). Box-Behnken design (BBD) was used to investigate the effects of various parameters affecting the adsorption of TCs onto Cs-PPy-Fe_3O_4 composite. The results displayed that the sorption of the TCs onto Cs-PPy-Fe_3O_4 composite followed pseudo-first-order and best fitted the Langmuir isotherm model with adsorption capacities of 112, 95, 94, and 93 mg g^{-1} for oxytetracycline, tetracycline, chlortetracycline, and doxycycline, respectively. Thermodynamic studies revealed that the adsorption of the analytes onto the Cs-PPy-Fe_3O_4 composite was physical with exothermic and increasing entropy. Furthermore, as the eluting solvent, the adsorbent could be regenerated using methanol and 0.01 oxalic acid (20:80 v/v). Therefore, the Cs-PPy-Fe_3O_4 composite could be a promising adsorbent for the simultaneous removal of TCs in water.

KEYWORDS

tetracyclines; box-behnken design; adsoption isotherms; kinetics; regeneration

Received: 28 June 2023, revised: 5 March 2024, accepted: 23 April 2024

INTRODUCTION

Drinking water is becoming extremely limited worldwide.[1] In 2017, the World Health Organization (WHO) reported that 10.5% of the global population (785 million) were deprived of clean drinking water, while 297,000 children under the age of 5 and 828,000 people die every year from diarrhoea-related diseases because of unsafe drinking water, poor sanitation and poor hygiene.[2] Furthermore, the world's population is continuing to rise, and it has been estimated that the world's population rose from 1 billion to nearly 7.6 billion in 2017. Additionally, it is estimated that by 2030 and 2050, the global population will increase to approximately 8.6 billion and 9.8 billion, respectively.[3] This increase in population will further result in increased water demand. It is further estimated that half of the world's population will be living in severe water stress by the year 2030.[4] The severe water stress is caused by, among other things, contamination of water by macro pollutants, inorganic chemicals (such as heavy metals), polycyclic aromatic hydrocarbons, microorganism and micropollutants (such as parabens, fragrances, and pharmaceuticals).[5]

Tetracyclines (TCs) are antibiotics frequently used as animal food additives and medicine for treating diseases. However, excessive use and lack of proper disposal and management of tetracyclines have resulted in their introduction into water resources, soil pollution, and bacteria gaining resistance.[6] The residues of antibiotics found in water bodies can be life-threatening to exposed humans due to their health effects as they can affect the development of teeth and bones, with an ability to cause hepatotoxicity.[7] Therefore, it is essential to monitor the occurrence of TCs in water bodies and develop their removal strategies in contaminated water. This is important considering that TCs are becoming prevalent in water bodies with recent data showing the presence of TC in groundwater with a concentration of 184 ng L^{-1}.[7] Amongst the treatment technologies developed for the remediation of TCs in water, adsorption has emerged as a method of choice due to its simple operation, cost-effectiveness, and high removal efficiencies.[8]

One of the mainstays of adsorption techniques in water treatment is the choice of adsorbent material, and various sorbents have been used. These adsorbent materials include zeolites,[9] activated carbon,[10] carbon nanotubes,[11] clays,[12] metal-organic frameworks[13] and polymers.[14] Among these adsorbents, activated carbon is the most frequently investigated sorbent in water and wastewater purification/treatment.[15] However, activated carbon has drawbacks, such as reduced selectivity and modification flexibility.[16] In recent years, the application of composite materials in treating water contaminated with antibiotics has emerged.[17-19] Composite materials can be produced from carefully selected chemicals and materials. Each contributes certain characteristics desired to complete the whole composite while enhancing the adsorption and removal of the targeted pollutants. For instance, in the preparation of a polypyrrole-iron oxide nanocomposite for the treatment of pharmaceuticals in water, the incorporation of iron oxide nanoparticles[20] was found to enhance the processability of polypyrrole (PPy) substrates[21] because PPy is an insoluble granular material made of intractable brittle thin films.[22] Although the incorporation of iron oxide nanoparticles may improve the processability of the PPy conducting polymer and thus its adsorption performance and removal of pollutants, PPy-Fe_3O_4 nanocomposites have low adsorption capacity.[23] This could be due to the tendency of Fe_3O_4 to form aggregation owing to their high surface energy.[24] Iron oxide nanoparticles are encapsulated inside a polymer to mitigate this drawback. Recently studies reported the application of chitosan-polypyrrole-iron oxide (Cs-PPy-Fe_3O_4) nanocomposite adsorbent in removing carbamazepine, chromium, and naproxen from water. [25-27] In these studies, including chitosan aided the encapsulation of Fe_3O_4 and thus mitigating the agglomeration while enhancing the removal performance.[25-27]

*To whom correspondence should be addressed
Email: pnnomngongo@uj.ac.za

ISSN 1996-840X Online / South African Chemical Institute / https://saci.co.za/journal

https://doi.org/10.17159/0379-4350/2024/v78a24

However, to our knowledge, no work has been published on employing Cs-PPy-Fe_3O_4 composite to remove tetracyclines (TCs) from wastewater. Furthermore, even though the adsorbent has been used for the removal of other contaminants,[25-27] it is important to demonstrate that the proposed adsorbent can be used for a wide range of pollutants that have multiple acid dissociation constants, thus making it a versatile adsorbent. Therefore, in this study, the Cs-PPy-Fe_3O_4 composite was synthesized via the facile co-precipitation method and applied as a suitable adsorbent for the removal of TCs in water. The adsorbent was characterized using various analytical techniques. The prepared composite was investigated for simultaneous adsorptive removal of oxytetracycline (OT), tetracycline (TC), chlortetracycline (CT), and doxycycline (DC) from aqueous environments. The effects of the most important parameters on the adsorption of TCs (mass of adsorbent, sample pH, contact time, initial concentration, and temperature) were investigated and optimized using response surface methodology (RSM) based on Box-Behnken design (BBD). The sorption data were examined using isotherms, kinetics, and thermodynamic models. The reusability of the adsorbent was investigated by performing several adsorption-desorption cycles.

EXPERIMENTAL

Materials

All chemicals in this study were analytical-grade reagents, and they were used as they were obtained. The analytes; tetracycline (purity = 98-102%), oxytetracycline dehydrate (purity = 95-102%), chlortetracycline (purity ≥ 91%), doxycycline monohydrate (purity = not given) were purchased from Merck, Johannesburg, South Africa. Acetonitrile (ACN) and methanol (MeOH)) were HPLC-grade solvents purchased from Merck, Johannesburg, South Africa. Chemical reagents such as hydrochloric acid (HCl), iron (III) chloride hexahydrate ($FeCl_3.6H_2O$), ammonium persulfate (APS), iron (II) tetrahydrate ($FeCl_2.4H_2O$), pyrrole, chitosan, sodium hydroxide (NaOH), oxalic acid dihydrate (OA), acetic acid (purity = 99%) were purchased from Merck, Johannesburg, South Africa. All aqueous solutions were prepared using 18 MΩ cm^{-1} resistivity ultrapure water (type 1, (Millipore, Bedford, MA, USA).

Preparation of adsorbents

Synthesis of chitosan-Fe_3O_4 composite

The synthesis of the chitosan-Fe_3O_4 composite was prepared by a co-precipitation method modified from Liao et al.[28] Briefly, 1.0 g chitosan was dissolved in 400 mL of 0.25% (v/v) acetic acid, followed by adding 30 mM $FeCl_3.6H_2O$ and 15 mM $FeCl_2.4H_2O$. The mixture was stirred for 1 h at 40 °C under inert conditions. Thereafter, 10% NaOH was added dropwise to adjust the pH of the solution to 10 under vigorous stirring. The solution was left to stir for an additional 1 h to form a black precipitate, which was collected using an external magnet. The residue was washed with ultrapure water and methanol several times and oven-dried at 60 °C overnight. The same procedure prepared iron oxide nanoparticles without the addition of Cs.

Synthesis of chitosan-polypyrrole-Fe_3O_4 composite

The synthesis of chitosan-polypyrrole-Fe_3O_4 (Cs-PPy-Fe_3O_4) composite was carried out as follows; 2.5 mL pyrrole monomer and 4 g of magnetic chitosan were added to a round flask containing 100 mL Milli-Q water. The mixture was stirred for 1 h at room temperature under a nitrogen atmosphere, then added 20 mL APS. The mixture was stirred for 4 h at room temperature. The black precipitate was collected with an external magnet and washed several times with Milli-Q water and methanol until the filtrate became colorless. The Cs-PPy-Fe_3O_4 composite was dried at 60 °C for 24 h. Synthesis of PPy followed the same procedure without adding the magnetic chitosan.

Instrumentation

The microscopic morphology, size, shape, and elemental analysis were evaluated using scanning electron microscopy (SEM, TESCAN VEGA 3 XMU, LMH instrument, Czech Republic) coupled with the energy dispersive X-ray spectroscopy (EDS) at a voltage of 20 kV. The internal structure of the composite was investigated by transmission electron microscopy (TEM JOELJEM 2100, Japan) at a voltage of 120 kV. The functional groups present in the materials were determined by using FTIR (KBr disk technique), model, and 100 FTIR spectrometer procured at PerkinElmer (Waltham, MA, USA) in the range 400 – 4000 cm^{-1}). The X-ray diffraction (XRD) analyses were performed on a PANalytical X'Pert X-ray Diffractometer (PANalytical BV, Netherlands) using a Cu K α radiation (λ = 0.15406 nm) in the 2θ range of 4–90° at room temperature to investigate the crystalline nature of the composite. Brunauer-Emmett-Teller (BET) was used to investigate the surface porosity of the individual components (Cs and Fe_3O_4 particles) and the composite by the multipoint method using the surface area and porosity analyzer (ASAP2020 V3, 00H, Micromeritics Instrument Corporation, Norcross, USA). The pH of the samples was adjusted using an OHAUS starter 2,100 pH meter (Pine Brook, NJ, USA). The concentrations of TCs were quantified using Agilent HPLC 1200 infinity series coupled with a diode array detector (Agilent Technologies, Waldbronn, Germany). The analytes were detected at two wavelengths (351 and 365 nm). The choice was based on the fact that TCs are being recorded in the range of 350-365.[29]An Agilent Zorbax Eclipse Plus C18 column (3.5 µm × 150 mm × 4.6 mm) (Agilent, Newport, CA, USA) was used to separate the analytes. The column temperature was kept at 25 °C, and the elution flow rate was 1.00 mL min^{-1}. The gradient elution using methanol (A), acetonitrile (B), and 0.03 M oxalic acid solution (C) was applied starting with 0:8:92(v/v/v) (A:B: C), which changed to 0:18:82 in 2 min and to 5:20:75 in 0.1 min which stayed isocratic for 4.9 min, and then changed to 10:25:65 for 3 min, then changed to 15:20:65 in 1 min and lastly to 15:25:60 in 3 min and stayed isocratic for 2 min then returning to the initial conditions in 3 min.[33] Origin 2018 Software was used for fitting and plotting data for isotherms and kinetic studies.

Adsorption experiments

To determine the adsorption capacity, the synthesized Cs-PPy-Fe_3O_4 composite was used as the adsorbent to remove TCs in water. The pH of aqueous solutions was adjusted with either diluted HCl or NaOH. Box-Behnken design (BBD) was used to optimize the batch adsorption process. The investigated parameters and their levels are shown in Table 1. Briefly, 15-30 mg of Cs-PPy-Fe_3O_4 samples were added into conical flasks with the desired TCs concentration (2 mg L^{-1} for each compound), sample pH (4-10), and volume (100 mL) of the solution. The solution was sonicated (5-60 min), followed by separating the supernatant from the adsorbent with an external magnet. After that, 1 mL of the supernatant was filtered through a 0.22 µm PVDF filter and analyzed using HPLC-DAD. The adsorption removal efficiency (%RE) was evaluated as follows:

$$\%RE = \frac{(C_0 - C_e)}{C_0} \times 100 \quad (1)$$

where C_0 and C_e (mg L^{-1}) are the initial and equilibrium concentrations, respectively.[30]

Post optimisation, the optimum experimental conditions were used to study the equilibrium isotherms and adsorption kinetics. Model solutions containing OT, TC, CT and DC at concentration levels ranging from 3-50 mg L^{-1} were used to perform equilibrium studies. The experiments were carried out in duplicate, and the adsorption capacities for OT, TC, CT and DC were determined by equation 2:

$$q_e = \frac{(C_0 - C_e)V}{m} \quad (2)$$

where C_0 and C_e (mg L^{-1}) are the initial and equilibrium concentration, respectively; V (L) is the volume of the solution and m (g) is the mass of Cs-PPy-Fe_3O_4 composite.[31]

Kinetic studies were carried out by adding 100 mL of a mixture of TCs (7 mg L^{-1} for each TC) into conical flasks and sonicated for 5 to 60 min. This was followed by the separation of the supernatant from the adsorbent by an external magnet. The supernatant was filtered and analysed by HPLC-DAD. The adsorption capacity was calculated at the time, t, (qt).

Regeneration and reusability

The reusability and regeneration capabilities of the Cs-PPy-Fe_3O_4 composite were investigated by performing five adsorption/desorption experimental cycles of the TCs. A desorption solvent containing a mixture of MeOH and 0.01 OA (20:80 v/v) was used to desorb TCs from the TC-loaded Cs-PPy-Fe_3O_4 adsorbent. The desorption experiments were done at room temperature through sonication of the adsorbent for 5 min. An external magnet separated the eluent and adsorbent. The eluent was then filtered and analysed using HLPC-DAD. After desorption, the composite was washed several times with Milli-Q water and dried at 60 °C for 2 h.

Collection of real samples

The composite prepared in this study was evaluated for its ability to adsorb the four TCs in wastewater. Both wastewater influent and effluent samples were collected from a local wastewater treatment plant, and preserved through keeping in coolerbox packed with ice during the transportation to the laboratory. The samples were filtered and the presence of TCs was monitored using HPLC. All the analytes were not detected in the samples. Therefore, spiking of both the influent and effluent samples with the TCs was performed prior to performing the adsorption studies.

RESULTS AND DISCUSSION

Characterisation

FTIR analysis

The FTIR spectra of Cs-Neat, Fe_3O_4-Neat and Cs-PPy-Fe_3O_4 are presented in Figure 1. Figure 1A shows chitosan characteristics peaks at 3423 cm^{-1}, 2850 cm^{-1} and 1053 cm^{-1} assigned to O-H/N-H, C-H and C-O-C stretching vibrations, while 1633 cm^{-1} and 1385 cm^{-1}were ascribed to N-H and C-H bending vibrations.[32] Iron oxide had characteristic peaks (Figure 1B) at 3352 cm^{-1} corresponding to O-H stretching vibration and 592 and 458 cm^{-1} corresponding to Fe-O stretching vibration.[33,34] The spectrum of PPy (Figure 1C) showed a

Table 1. Factors and levels used in the Box-Behnken design.

Factors	Low level	Central point	High level
Mass of adsorbent (MA, mg)	15	22.5	30
pH	4	7	10
Contact time (cT, min)	5	33	60

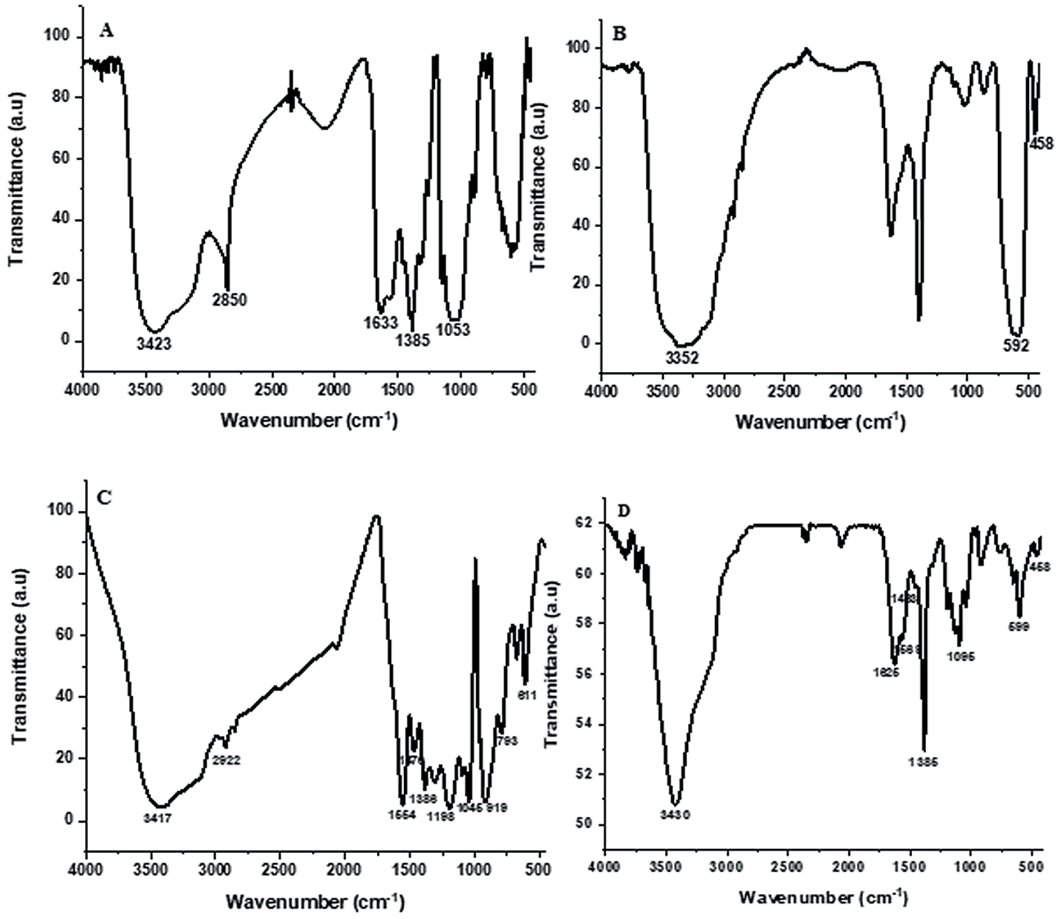

Figure 1. FTIR spectra of a) Cs, b) Fe_3O_4-Neat c) PPy and d) Cs-PPy-Fe_3O_4 composite.

broad peak at 3417 cm^{-1} due to the N-H stretching vibrations, while the peak at 2922 cm^{-1} was attributed to the C-H stretching vibrations.[35] The peaks at 1554 and 1470 cm^{-1} were ascribed to the C=C stretching vibrations of the PPy ring.[36] The peak at 1386 cm^{-1} corresponded to the C-N stretching vibrations.[37,38] The peak at 1198 cm^{-1} was due to C-N stretching vibrations.[39] The peak observed at 1045 corresponds to C-H in-plane bending vibrations.[39] The 919 and 793 cm^{-1} peaks are ascribed to C-H out-of-plane vibrations.[40,41] The peak at 611 cm^{-1} was due to the in-plane deformation of the ring.[42] The spectrum of the Cs-PPy-Fe_3O_4 composite (Figure 1D) showed a peak at 3430 $cm^{-1,}$ which resulted from O-H and N-H stretching vibrations of both Cs and PPy. Characteristic peaks of Cs observed at 1633 and 1053 cm^{-1} in the Cs spectrum shifted to 1625 and 1095 $cm^{-1,}$ respectively, in the Cs-PPy-Fe_3O_4 spectrum. The 2922 and 2850 cm^{-1} peaks for PPy and Cs disappeared in the Cs-PPy-Fe_3O_4 spectrum. The peaks at 1569 and 1463 cm^{-1} are due to PPy. Finally, the peaks 599 and 458 cm^{-1} are ascribed to Fe-O stretching vibration, confirming the presence of iron oxide nanoparticles in the composite. Therefore, the results suggested that the Cs-PPy-Fe_3O_4 composite was successfully synthesised.

XRD analysis

Figure 2 illustrates the XRD patterns of Cs, Fe_3O_4 (JCPDS card number 04-013-9809), PPy and Cs-PPy-Fe_3O_4 composite. The XRD pattern of Cs (Figure 2A) showed sharp narrow peaks at 2θ angles 10.2° and 20.0°, characteristic of crystallinity in Cs biopolymer.[43] The broad peak at 2θ angle 41.1°characterised the amorphousness of the Cs biopolymer.[44] Characteristic peaks associated with Fe_3O_4 in Figure 2B agreed with previous studies.[45,46] A broad peak for PPy (Figure 2C) was observed at an angle of 24.7°, corresponding to the amorphous region of PPy,[47] while the peak at 43.5° was possibly due to impurities. From the Cs-PPy-Fe_3O_4 composite (Figure 2D), the characteristic peaks associated with the crystalline Fe_3O_4 phase can be seen. Furthermore, the peak at 24.7° corresponds to PPy.

TEM, SEM and EDS analysis

The morphologies of the Fe_3O_4 particles and Cs-PPy-Fe_3O_4 composite were investigated by TEM and SEM (Figure 3). The TEM image in Figure 3(A) showed that the Fe_3O_4 particles were semi-spherical and aggregated, which agreed with the results of a different study.[48] The TEM image in Figure 3(B) showed that the Fe_3O_4 particles were dispersed in the polymer matrix.[49] However, aggregation was still visible.

Scanning electron microscopy images in Figure 4 (A and C) showed that chitosan and iron oxide displayed a lamellar structure. The polypyrrole and the composite were composed of nodular structures (Figures 4B and 4D).[50] The composite was more porous than the individual components (Cs and Fe_3O_4), which could be attributed to PPy chain agglomerates covering the Cs and Fe3O4 particles, increasing the porosity.[51] The EDS analysis of the individual components (chitosan, polypyrrole and iron oxide) is presented in Figure S1. The EDS analysis of the composite (Figure 4E) confirmed the presence of chitosan and polypyrrole due to the detection of C (53.6%), O (18.0%) and N (12.4%) peaks. The Fe (12.4%) and O (18.0%) peaks further confirmed the incorporation of iron oxide. The S and Cl peaks in the composite were due to the ammonium persulfate and iron salts during the synthesis step.

BET analysis

To investigate the surface area and porosity of the composites, N_2 adsorption/desorption experiments were carried out, and the results are illustrated in Table 2. From the results, Cs, Fe_3O_4 particles and

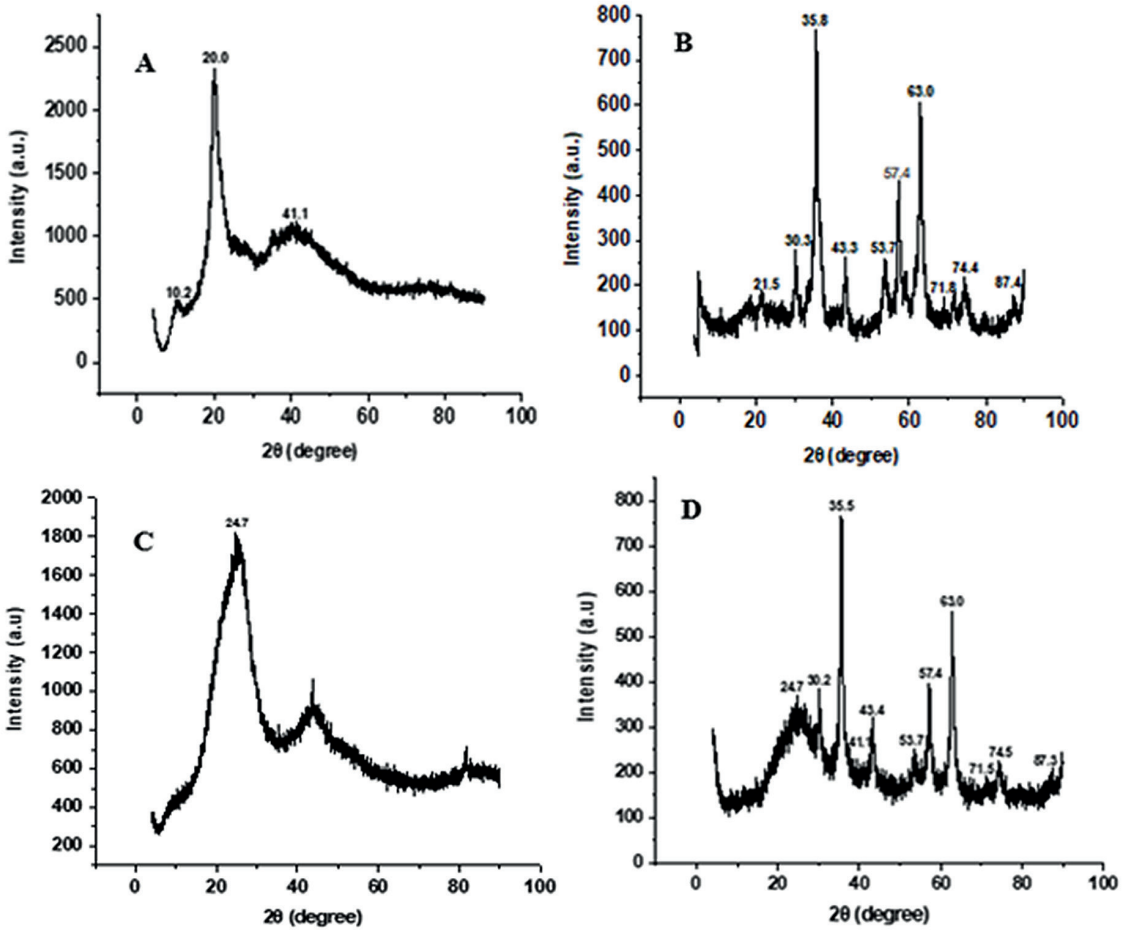

Figure 2. XRD spectra of a) Cs, b) Fe_3O_4-Neat c) PPy and d) Cs-PPy-Fe_3O_4 composite.

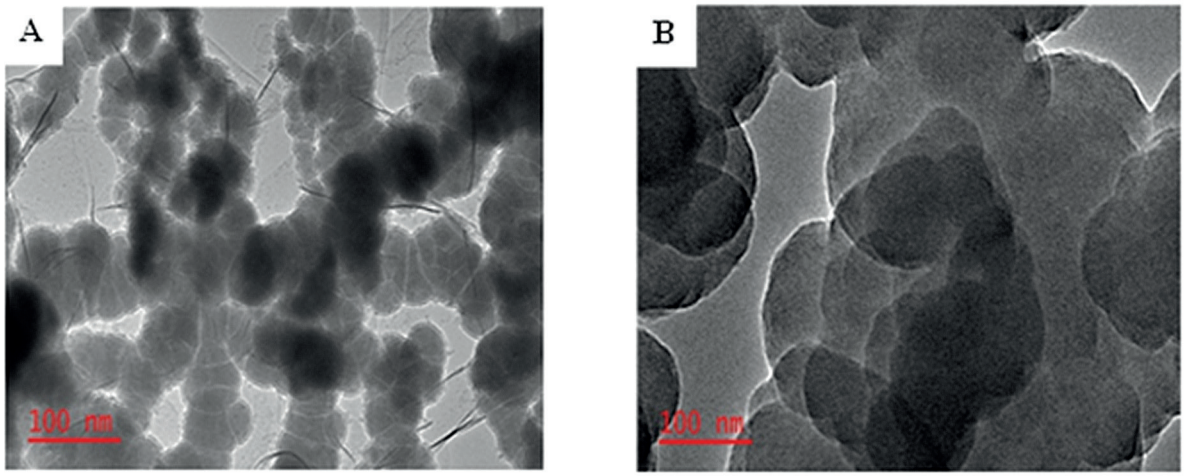

Figure 3. TEM image of A) Fe_3O_4-Neat, B) Cs-PPy-Fe_3O_4 composite.

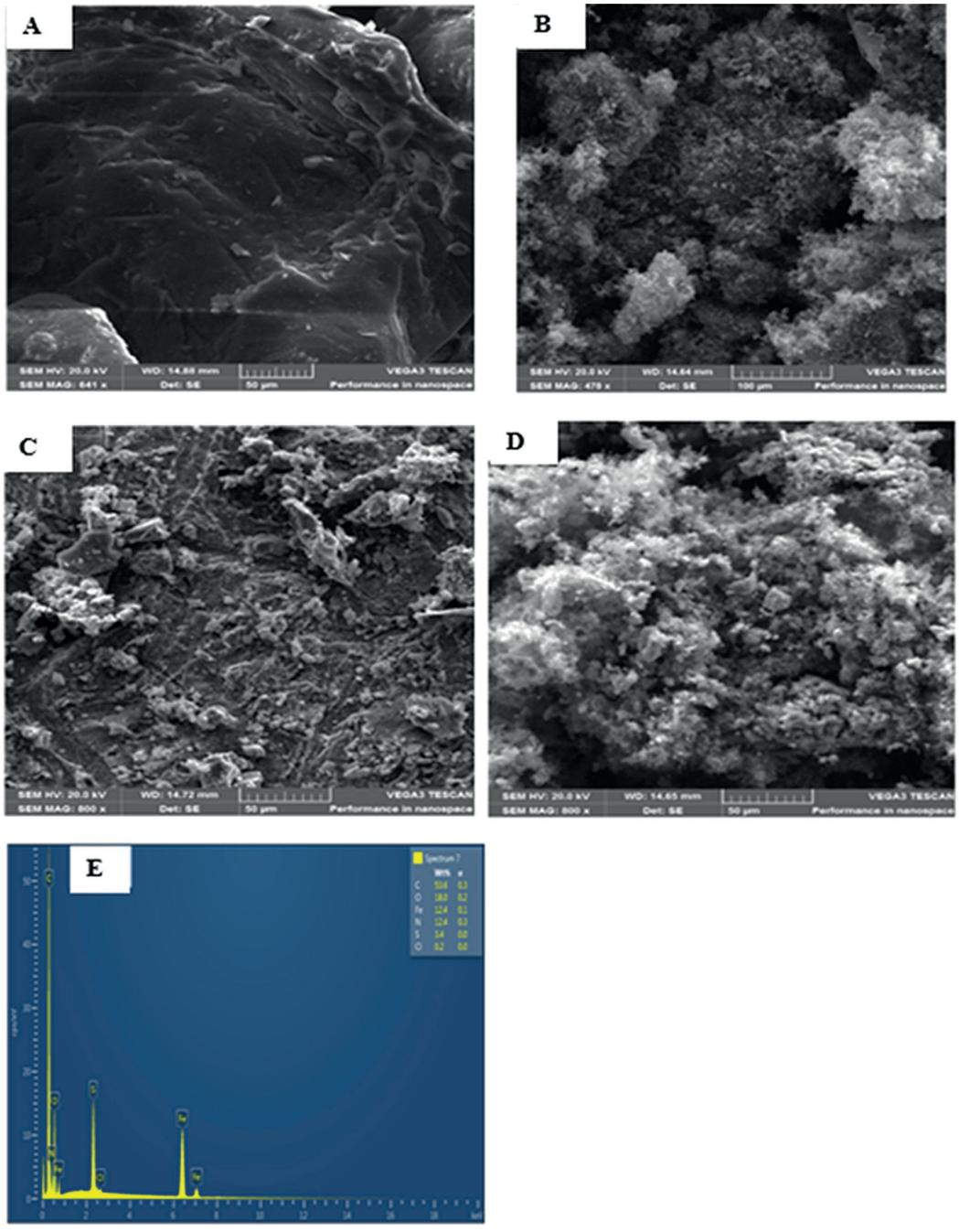

Figure 4. SEM image of A) Cs, B) PPy, C) Fe_3O_4-Neat, D) Cs-PPy-Fe_3O_4 and E) EDS spectrum of Cs-PPy-Fe_3O_4 composite.

Cs-PPy-Fe_3O_4 composites had surface areas of 0.3276, 13.8 and 129.4 $m^2\ g^{-1,}$ respectively. Iron oxide and the Cs-PPy-Fe_3O_4 composite had pore volumes of 0.03 and 0.32 $cm^3\ g^{-1,}$ respectively, while the pore sizes were 7.6 and 9.9 nm, respectively. The results show that the BET surface area, pore volume and pore size of the Cs-PPy-Fe_3O_4 composite were higher than those of Cs and Fe_3O_4 particles. This means the synthesis of the composite improved these features, which could be beneficial for the application of the resulting material as an adsorbent.

Optimisation of adsorption parameters

Optimisation by Box-Behnken design

The batch adsorption optimisations were carried out using the Box-Behnken design; the results are shown in Table S1. The analysis of variance (ANOVA) was used to analyse the statistical significance of the investigated independent factors on removal efficiency at the 95% confidence level. The ANOVA results were reproduced as Pareto charts. Only the linear factors (indexed L) were considered during the Pareto charts' analysis, while quadratic factors (indexed Q) were excluded (Figure 5). This is due to the ANOVA being a linear model. The results in Figure 4 showed that the factors with significant effects were sample pH for all analytes of interest and mass of adsorbent (MA) for OT. This suggests that these independent factors were more influential on the analytical response.

Response surface methodology (RSM)

The 3D response surface plots were used to study the combined effects of the factors on the removal of OT, TC, CT and DC from water. The results from Figure 6 (A and B) show that maximum concentration was observed when the sample pH was between 3.5 and 7.5 and with any amount of MA and cT. This might be attributed to the sample pH affecting the TCs' ionisation and the adsorbent's surface charge.[52] The point of zero charges for Cs-PPy-Fe_3O_4 composite was determined to be 7.50 (Figure S2), suggesting that when the pH was below the pH_{pzc}, the adsorbent surface was positive and conversely, when the sample pH was above the pH_{pzc} the surface of the adsorbent was negative. All TCs have three disassociation constants; namely, pKa_1 = 3.2, pKa_2 = 7.5 and pKa_3 = 8.9 for OT, pKa_1 = 3.3, pKa_2 = 7.8 and pKa_3 = 9.6 for TC, pKa_1 = 3.3, pKa_2 = 7.6 and pKa_3 = 9.3 for CT and pKa_1 = 3.0, pKa_2 = 7.9 and pKa_3 = 9.2 for DC.[53] TCs are cationic when pH < pKa_1, zwitterionic when $pKa_1 \leq pH \leq pKa_2$ and anionic when pH > pKa_2.[54] The maximum concentration was seen when the sample pH was between 3.5 and 7.5 was due to the electrostatic interactions between the zwitterionic species of the TCs and positively charged Cs-PPy-Fe_3O_4 surface. Figure 6C shows the interaction between MA and cT. In this case, maximum concentration was observed when MA was below 19 mg and cT was between 1 and 70 min. The opposite effect was observed when the MA was above 19 mg. This could be attributed to the increase in the number of analyte binding sites. However, increasing the mass of the adsorbent may have resulted in the agglomeration of particles and thus decreased the surface area.[55]

Table 2. Summary of the BET analysis for Cs, Fe_3O_4 and Cs-PPy-Fe_3O_4 composite.

Parameters	Cs	Fe3O4	Cs-PPy-Fe3O4
BET surface area (m2 g-1)	0.3276	13.8	129.4
Total pore volume (cm3 g-1)	-	0.03	0.32
Pore size diameter (nm)	-	7.6	9.9

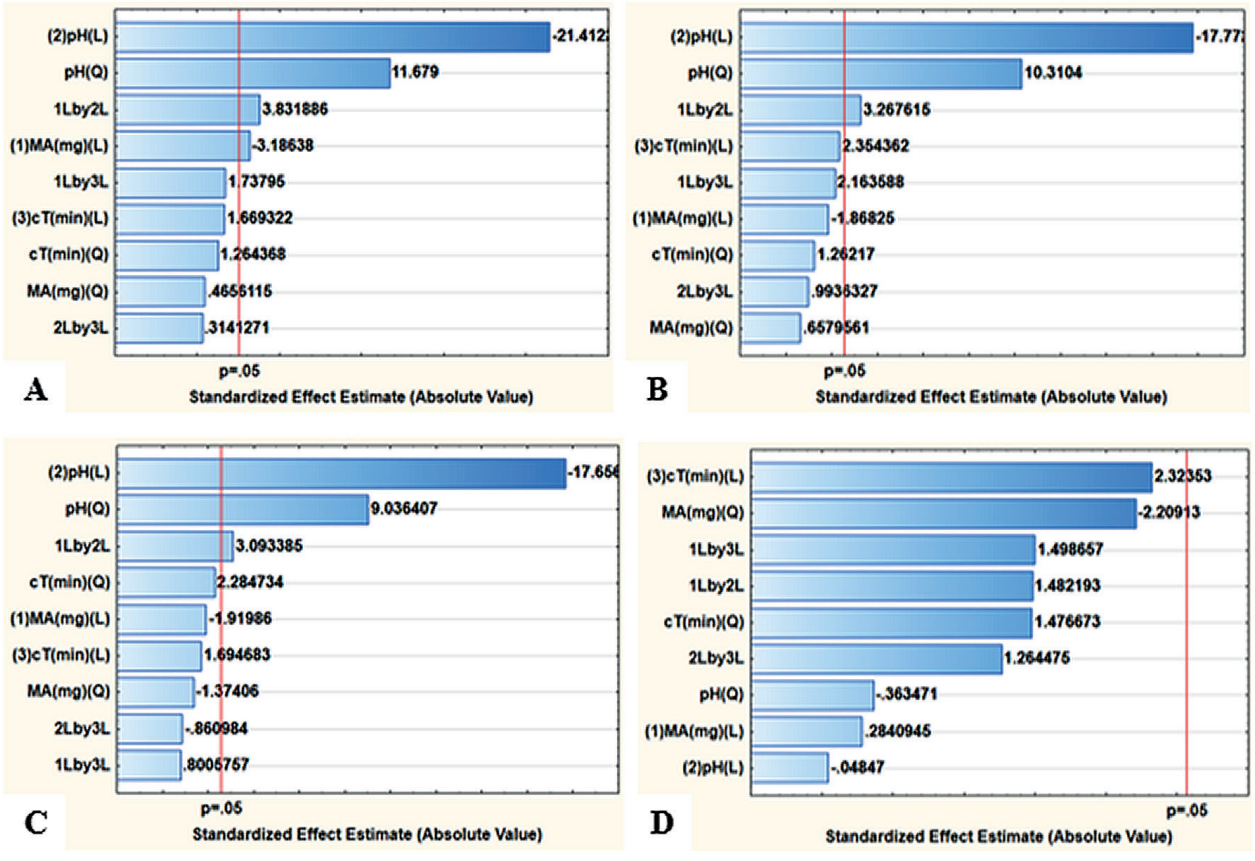

Figure 5. Pareto chart of standardised effects for adsorption of (A) OT, (B) TC, (C) CT and (D) DC. MA: mass of adsorbent, pH: sample pH, cT: contact time, 1Lby2L: indicates the interaction between MA and pH, 1Lby3L: interaction between MA and cT, 2Lby3L: interaction between pH and cT.

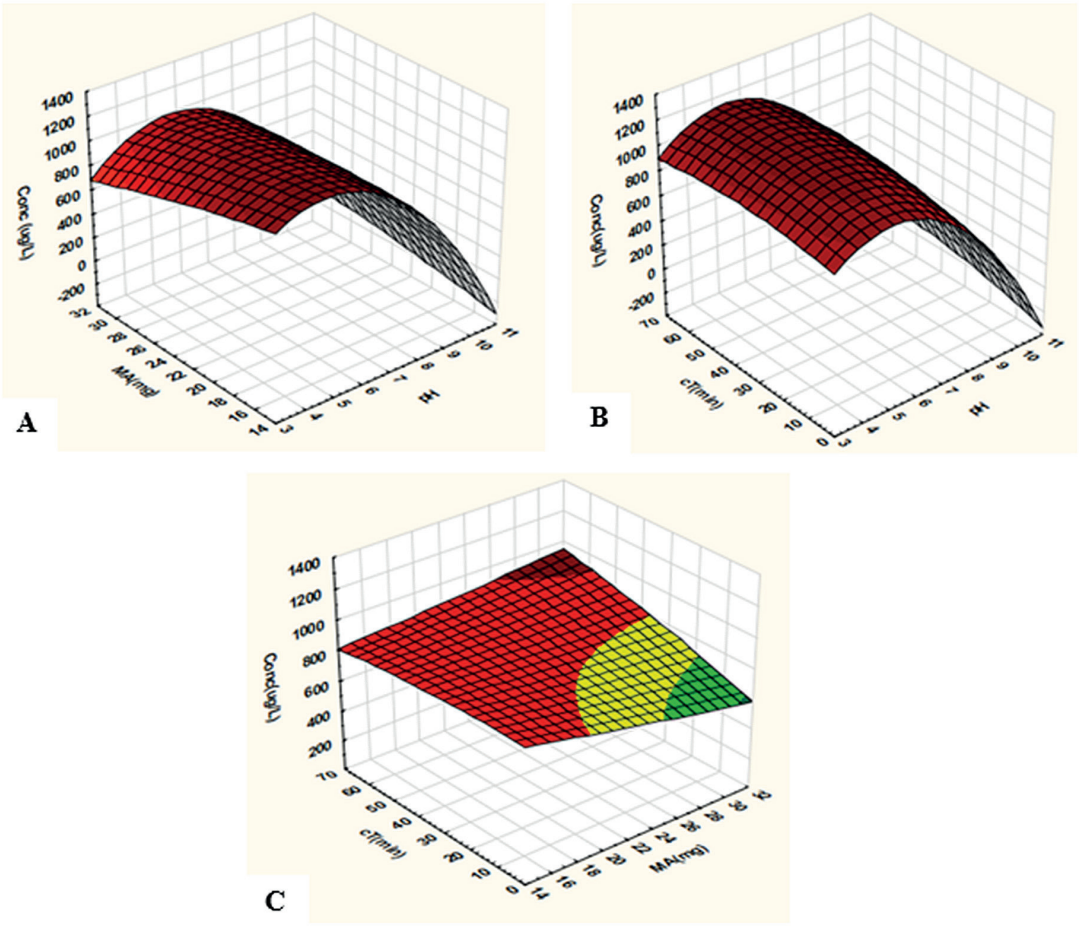

Figure 6. 3D response surface plots illustrating the investigated factors' combined interactive effects. Interactions (A) between sample pH and MA; (B) between sample pH and cT and (C) between MA and cT.

Desirability function

Using the desirability function permits estimating the optimum values for the investigated factors. The results are illustrated in Figure 7. The optimum conditions for the removal process were 4, 15 mg and 5 min for sample pH, mass of adsorbent and contact time, respectively. Under optimal conditions, the predicted concentration for the adsorption of OT, TC, CT and DC were 917.01, 1211.2, 2661.7 and 1855.3 µg L^{-1}, respectively (Figure S3). These predicted optimal conditions were confirmed experimentally by performing the adsorption process five times. The experimental results gave concentrations of 913.9 ± 2.3, 1210.8 ± 3.7, 2634.9 ± 39.6 and 1857.4 ± 28.6µg L^{-1} for OT, TC, CT and DC, respectively.

Adsorption isotherms

Isotherm studies were conducted to determine the relationship between the remaining concentration of TCs after reaching equilibrium and the amount adsorbed onto the Cs-PPy-Fe_3O_4. This was achieved by fitting the data into five nonlinear isotherm models: Langmuir, Freundlich, Dubinin-Radushkevich, Hill and Sips. The Langmuir isotherm model indicates monolayer adsorption onto a homogenous surface.[56] The nonlinear equation of the Langmuir isotherm model is shown in equation (3):

$$qe = \frac{q_{max} K_L C_e}{1 + K_L C_e} \quad (3)$$

where qe (mg g^{-1}) is the amount of TCs adsorbed at equilibrium, Ce (mg L^{-1}) is the concentration of TCs at equilibrium and q_{max} (mg g^{-1}) and K_L (L mg^{-1}) are model parameters related to maximum adsorption capacity and free adsorption energy, respectively.[57] The adsorption equilibrium is favourable when K_L is greater than zero but less than one. When K_L is greater than one, the adsorption equilibrium is not favourable.

The Freundlich isotherm model indicates heterogeneous adsorption on the adsorbent's surface and that the adsorption heat is not uniform.[58] The nonlinear equation of the Freundlich isotherm model is given in equation (4):

$$qe = K_F C_e^{1/n} \quad (4)$$

where n shows the adsorption intensity and K_F (mg g^{-1})(L mg^{-1})$^{1/n}$ is the Freundlich constant, respectively. When n is greater than one, adsorption is favourable.[58]

Dubinin-Radushkevich (D-R) isotherm model assumes that the adsorption process is related to micropore volume filling rather than layer-by-layer adsorption on the pore walls. This model accounts for the effects of the porous structure of the adsorbent.[59] The nonlinear equation of the D-R isotherm model is given in equation (5):

$$qe = qDexp^{-(\beta\varepsilon 2)} \quad (5)$$

where β (mol^2 kJ^{-2}) is the D-R isotherm constant associated with the adsorption energy and ε (kJ mol^{-1}) is the adsorption potential.[60]

Hill isotherm model assumes that the adsorption process is a cooperative phenomenon of analytes on the adsorbent site affecting different adsorbent sites.[61] The nonlinear equation of the Hill isotherm model is given in equation (6):

$$qe = \frac{qHC_e^{n_H}}{KD + C_e^{n_H}} \quad (6)$$

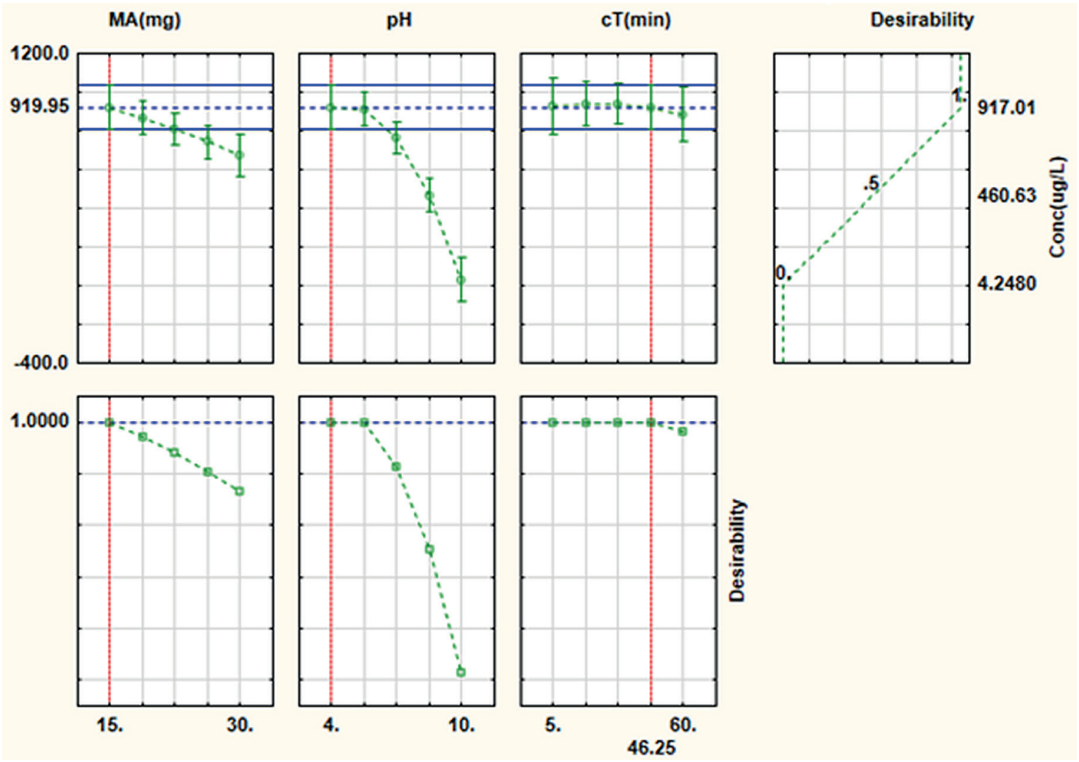

Figure 7. Profiles for predicted values and desirability function for the removal of TCs.

where n_H is the binding interaction coefficient, and K_D is the Hill isotherm constant.[62]

Sips isotherm model combines both Langmuir and Freundlich isotherms. The heterogeneity factor *nS* associated with this isotherm model is typically less than one, indicating a heterogeneous surface. When *nS* equals one, the equation reduces to Langmuir, indicating a homogeneous surface.[63] The nonlinear equation for the Sips isotherm model is shown in equation (7):

$$qe = \frac{qsKsC_e^{ns}}{1 + KsC_e^{ns}} \quad (7)$$

where q_s (mg g^{-1})is the maximum adsorption capacity, *nS* is the heterogeneity factor and K_s (L mg^{-1}) is the affinity constant.[64]

The nonlinear isothermal parameters and the correlation coefficients (R^2) for Langmuir, Freundlich, Dubinin-Radushkevich, Hill and Sips isotherms are shown in Table 3. From the results, the correlation coefficients for OT, TC, CT and DC for the Freundlich isotherm model were 0.9603, 0.9521, 0.9467 and 0.9649, respectively, with n_F of 2.56, 3.40, 2.21 and 2.53 for OT, TC, CT and DC, respectively. Since the values of $n_F > 1$, this suggested that adsorption was favourable.[65] The Langmuir isotherm model R^2 values were 0.9971, 0.9961, 0.9831 and 0.9877 for OT, TC, CT and DC, respectively, with maximum adsorption capacity of 112, 95, 94 and 93 mg g^{-1} for OT, TC, CT and DC, respectively. However, the results showed that the Langmuir isotherm model best fitted the experimental data since its R^2 value was higher than that of the Freundlich isotherm model. The results suggested a monolayer and homogenous adsorption of the TCs onto the Cs-PPy-Fe_3O_4 surface. The Sips isotherm model agreed with the results observed. As mentioned earlier, when ns equals 1, the model reduces to Langmuir, suggesting homogeneous adsorption. Furthermore, the Hill cooperativity coefficient constant (ns) was greater than 1, suggesting positive cooperativity in binding.

Adsorption kinetics

Kinetic studies are important since they provide useful information, such as a better understanding of the adsorption mechanism and the interaction between the adsorbent and the analytes.[66] The effects of time on the adsorption of TCs on Cs-PPy-Fe_3O_4 were investigated. This was accomplished by fitting the data into four kinetic models: pseudo first order, pseudo-second order, Elovich and intra-particle diffusion kinetic models. Pseudo-first order (PFO) assumes that the adsorption process is determined by diffusion from one layer to another.[56] The nonlinear equation for the PFO model is shown in equation (8):

$$qt = qe(1 - e^{-k1t}) \quad (8)$$

where qe (mg g^{-1}) is the amount of TCs adsorbed at equilibrium, qt (mg g^{-1}) is the amount of TCs at time t, k_1 (min^{-1}) is the first order rate constant, and t (min) is the adsorption time.[67]

Pseudo-second order (PSO) assumes the adsorption process is determined by chemical uptake.[56] The nonlinear equation for the PSO model is presented in equation (9):

$$qt = \frac{qe^2k_2t}{1 + qek_2t} \quad (9)$$

where k_2 (g mg^{-1} min^{-1}) is the second-order rate constant.[68]

Elovich model assumes that adsorption occurs in two steps, a quick initial reaction based on the movement of the analytes to available external sites followed by a slow diffusion of the analytes in and out of the adsorbent's micropores.[69] The nonlinear equation for the Elovich model is shown in equation (10):

$$q_t = \frac{1}{\beta}\ln(1 + \alpha\beta t) \quad (10)$$

where α (g mg^{-1}) is the desorption coefficient, and β (mg g^{-1} min^{-1}) is the adsorption rate.[70]

Intra-particle diffusion model assumes that the interaction of the adsorbate and the adsorbent is instantaneous relative to the diffusion steps, and therefore, these diffusion steps determine the overall rate.[71] The equation for the intra-particle diffusion model is shown in equation (11):

$$q_t = K_{id}t^{1/2} + C \quad (11)$$

where K_{id} (mg g^{-1} $min^{1/2}$) is the rate coefficient and C (mg g^{-1}) is the diffusion constant representing the thickness of the boundary layer.[72]

The results of the nonlinear fit for the pseudo-first order, pseudo-second order, Elovich and linear intra-particle diffusion kinetic models are shown in Table 4. From the results, the R^2 values for pseudo first order were 0.9978, 0.9988, 0.9967 and 0.9978 for OT, TC, CT and DC, respectively. While for the pseudo-second order, the R^2 values were 0.9960, 0.9972, 0.9944 and 0.9971 for OT, TC, CT and DC, respectively. The results from the models revealed that the adsorption of the analytes onto the adsorbent followed a pseudo first-order kinetic model since the R^2 values were greater than those of the other three models (pseudo-second order, Elovich model and intra-particle diffusion). This suggests that the adso rption of TCs onto Cs-PPy-Fe_3O_4 adsorbent may have been physical.[73] Elovich kinetics model did not fit better with the data due to lower R^2 values. This further validates that chemisorption was not the rate-determining step. To determine the rate-determining step, different intra-particle diffusion models were used. From the results in Table 4, a two-step adsorption process occurred, the first being film diffusion and the second being intra-particle diffusion. Since the plots for all the analytes did not go through the origin, this suggested that intra-particle diffusion was not the rate-determining step. K_{id1} for the film diffusion was greater than K_{id2} for intra-particle diffusion, suggesting that intra-particle diffusion was slow.

Adsorption thermodynamics

Thermodynamic studies became useful in determining the dominant adsorption mechanism. To evaluate thermodynamic factors such as the standard enthalpy (ΔH°), free energy (ΔG°) and entropy (ΔS°), adsorption experiments were carried out at three temperatures (298.15, 308.15 and 318.15 K). The Van't Hoffs equation (equation 12) was used to calculate the change in enthalpy and entropy, while the Gibbs free energy was determined using equation (13):

Table 3. Adsorption isotherm parameters for the adsorption of TCs onto Cs-PPy-Fe_3O_4 composite.

Isotherms	Parameters	OT	TC	CT	DC
Langmuir	q_{max}	112	94.7	94.4	92.9
	K_L	0.087	0.14	0.063	0.086
	R_L	0.19-0.79	0.12-0.69	0.24-0.84	0.19-0.79
	R^2	0.9971	0.9961	0.9831	0.9877
Freundlich	K_F	20.7	27.5	13.1	16.9
	n_F	2.56	3.40	2.21	2.53
	R^2	0.9603	0.9521	0.9467	0.9649
D-R	q_{D-R}	85.8	78.1	69.5	70.4
	E	0.17	0.24	0.14	0.18
	R^2	0.8849	0.8382	0.8939	0.8697
Hill	q_H	106.86	95.89	85.09	95.13
	n_H	1.1	1.1	1.2	1.1
	K_d	13.0	6.59	21.5	11.2
	R^2	0.9978	0.9962	0.9861	0.9878
Sips	q_S	109	95.6	91.5	92.8
	n_S	1.2	0.9	1.4	1.0
	K_S	0.12	0.12	0.11	0.09
	R^2	0.9977	0.9963	0.9848	0.9877

Table 4. Kinetic parameters for the adsorption of TCs onto Cs-PPy-Fe_3O_4 composite.

	Parameters	OT	TC	CT	DC
PFO	qexpt (mg g-1)	41.7	39.6	27.3	36.7
	qe (mg g-1)	47.3	44.3	32.9	42.5
	K1 (min-1)	0.0394	0.0403	0.0332	0.0357
	R2	0.9978	0.9988	0.9967	0.9978
PSO	qe (mg g-1)	66.5	61.9	48.2	60.8
	K2 (mg g-1 min-1)	4.76E-04	5.29E-04	5.12E-04	4.57E-04
	R2	0.9960	0.9972	0.9944	0.9971
Elovich	β (mg g-1 min-1)	0.0469	0.0509	0.0604	0.0499
	α (g mg-1)	2.46	2.40	1.32	1.94
	R2	0.9931	0.9945	0.9917	0.9955
Intra-particle diffusion	Kid1 (mg g-1 min1/2)	12.8	12.2	8.10	10.9
	C1 (mg g-1)	3.26E-10	3.95E-11	2.92E-12	2.13E-12
	R2	0.6759	0.6826	0.6333	0.6764
	Kid2 (mg g-1 min1/2)	0.41	6.37	1.54	2.38
	C2 (mg g-1)	40.5	21.9	23.1	30.1
	R2	0.9838	0.9730	0.9410	0.8289

$$\ln(K) = \frac{\Delta S^\circ}{R} - \frac{\Delta H^\circ}{RT} \quad (12)$$

$$\Delta G^\circ = -RT \ln K \quad (13)$$

where T (K) is the temperature of the solution, R (J mol^{-1} K) is the universal gas constant, and K is the thermodynamic equilibrium constant of the adsorbent equal to q_e/C_e.[74]

The slope and intercept of the Van't Hoff plot of ln K versus 1/T were used to calculate ΔH° and ΔS° respectively, and equation 13 was used to calculate ΔG° and the results are presented in Table 5. The negative values of ΔG° reveal that the adsorption of the TCs onto the Cs-PPy-Fe_3O_4 composite was spontaneous and thermodynamically favourable. Furthermore, when the values of ΔG° are between -20 and 0 kJ mol^{-1}, this suggests a physical adsorption process.[75] Since ΔG° values for all four analytes were between -20 and 0 kJ mol^{-1}, a physical process governed the removal of TCs in water. These results agree with kinetic studies (Section 3.4) that showed that the experimental data best fitted the pseudo-first order model. The negative values of ΔH° indicate that the adsorption process was exothermic. The positive values of ΔS° suggested an increase in the randomness at the solid-solution interface during the adsorption process.

Possible adsorption mechanism

To gain insight into the adsorption mechanism of OT, TC, CT, and DC onto the Cs-PPy-Fe_3O_4 composite, the composite was characterised by FTIR before and after adsorption, and the results are presented in Figure 8 A and B, respectively. The possible adsorption mechanism is depicted in Figure 9. The adsorption of the TCs could be attributed to cationic-π bonds, hydrogen bonding, π–π interactions and electrostatic interactions. Cationic-π bonds could have occurred between the electron-rich benzene ring of the TCs and the protonated amino groups of the adsorbent and vice versa. This is evident in the FTIR spectrum of Cs-PPy-Fe_3O_4 after adsorption; the peaks at 3430 and 1625 cm^{-1} shifted to 3493 and 1613 cm^{-1}, respectively. At the same time, hydrogen bonding could have occurred between the OH from the adsorbent with the OH from the TCs. This can be seen by the peak shift from 3430 to 3493 cm^{-1}. Another possible contribution of TCs adsorption was due to π–π interactions between the benzene ring of the TCs and that of the adsorbent. The disappearance can see of the peaks at 1569 and 1463 cm^{-1} after adsorption. Finally, electrostatic interactions between the analytes' oxygen-rich functional groups and the adsorbent's protonated amino groups might have occurred. The overall results suggest that the adsorption process was physical adsorption.

Comparison of proposed adsorbent with other adsorbents for TCs removal

The performance of the Cs-PPy-Fe_3O_4 composite was compared with other reported adsorbents for the removal of TCs by looking at the adsorption capacity and the isotherm model followed, and the results are presented in Table 6. The Cs-PPy-Fe_3O_4 composite performed better than magnetic graphene, MIP composite and the EGA_{NaCl}. However, the activated carbon and biochar performed better than the Cs-PPy-Fe_3O_4 composite. These results indicate that the Cs-PPy-Fe_3O_4 composite can serve as a promising adsorbent for the removal of TCs.

Regeneration and reusability

It was essential to evaluate the regeneration of the adsorbent to investigate the stability and reusability of the adsorbent. The use of Cs-PPy-Fe_3O_4 composite using a mixture of MeOH and 0.01 OA (20:80 v/v) was repeated five times. It was evident that the removal efficiency of the TCs decreased by approximately 2% with the increase in the number of recycles. However, the removal efficiency still was above 65% after five cycles. These results showed that the Cs-PPy-Fe_3O_4 composite could be regenerated and recycled and maintain good adsorption properties.

Application to real samples

The prepared composite's feasibility was evaluated for removing OT, TC, CT and DC from wastewater samples (influent and effluent wastewater). The samples were filtered before analysis followed by

Table 5. Thermodynamic parameters for TCs adsorption onto Cs-PPy-Fe_3O_4 composite.

Analytes	T (K)	ΔG° (kJ mol-1)	ΔH° (kJ mol-1)	ΔS° (J mol K-1)
OT	298.15	-8.85	-5.57	10.98
	308.15	-8.92		
	318.15	-9.07		
TC	298.15	-8.20	-5.60	8.71
	308.15	-8.27		
	318.15	-8.38		
CT	298.15	-5.14	-2.10	10.22
	308.15	-5.25		
	318.15	-5.34		
DC	298.15	-6.83	-2.62	14.09
	308.15	-6.96		
	318.15	-6.11		

Table 6. Comparison of the adsorption capacity of TCs with various adsorbents.

Analyte (s)	Adsorbent	Adsorption capacity (mg g-1)	Isotherm model	Ref
OT, TC, CT and DC	Graphene functionalised magnetic particles	35.5–45.0	Langmuir	[76]
OT, TC, CT and DC	Molecular imprinted polymer composite	9.2–98.0	Freundlich	[77]
OT and DC	EGA_{NaCl}	4.2 & 4.5	Freundlich	[78]
OT, CT and DC	Mesoporous activated carbon	137.0–909.1	Langmuir	[79]
OT, TC and CT	Biochar	129.9–200.0	Langmuir	[80]
OT, TC, CT and DC	Chitosan-polypyrrole-iron oxide composite	94.4–112.3	Langmuir	This study

determination of TCs before and after adsorption and the results are summarised in Table 7. From the results, none of the analytes were detected in the wastewater samples prior to analysis. However, different concentrations spiked the wastewater samples with the target compounds. This was essential to determine if the developed analytical method could remove and detect the investigated compounds in real water samples. The removal efficiencies of OT, TC, CT and DC in spiked wastewater samples ranged between 88.7-98.5%. The results illustrated that good removal efficiencies were obtained, indicating a good performance by the Cs-PPy-Fe_3O_4 composite in removing TCs. This suggested that the composite has great potential for application in water treatment.

CONCLUSION

The current study prepared and characterised the Cs-PPy-Fe_3O_4 composite using FTIR, XRD, TEM, SEM and EDS techniques. The adsorption capabilities of the Cs-PPy-Fe_3O_4 composite were investigated for removing TCs in aqueous solutions.. The results revealed that the Langmuir isotherm model with an adsorption capacity of 112, 95, 95 and 93 mg g^{-1} for OT, TC, CT and DC, respectively, fitted the experimental data best. Thermodynamic studies revealed that adsorption was spontaneous, favourable, exothermic, and physisorption-driven. Kinetic studies that adsorption was well described by the pseudo-first order, further confirming that adsorption was driven by physical adsorption. The overall results suggested that the adsorption of TCs was through physical adsorption. The proposed adsorption mechanism was through cationic-π bonds, hydrogen bonding and π–π interactions. The removal efficiency of the TCs remained above 65% after five cycles.

ACKNOWLEDGEMENTS

This research was supported by the National Research Foundation (NRF, grant no. 91230) and the University of Johannesburg for making this research possible by providing laboratory facilities.

SUPPLEMENTARY MATERIAL

Supplementary material for this article can be found in the online supplemental pdf.

CONFLICT OF INTEREST

The authors declare no conflict of interest.

ORCID IDS

Mpho C. Lefatle: https://orcid.org/ 0000-0003-2251-4486
Lawrence M. Madikizela: https://orcid.org/0000-0001-6096-2701
Vusumzi E. Pakade: https://orcid.org/0000-0003-4228-6417
Philiswa N. Nomngongo: https://orcid.org/0000-0001-7615-0548

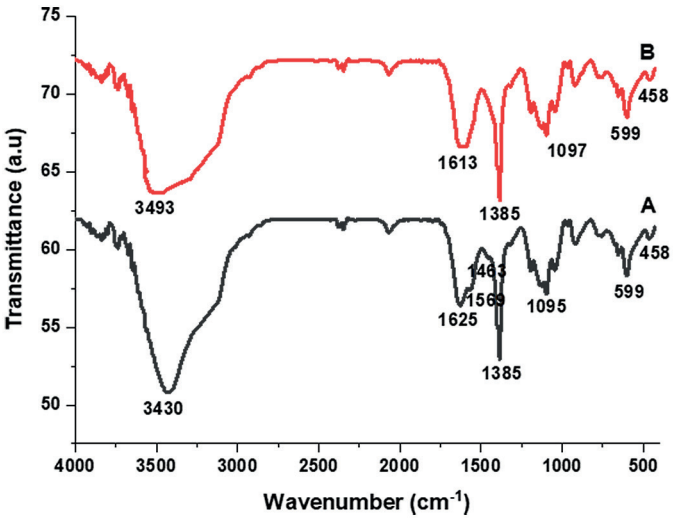

Figure 8. FTIR spectra of Cs-PPy-Fe_3O_4 A) before adsorption and B) after adsorption of TCs.

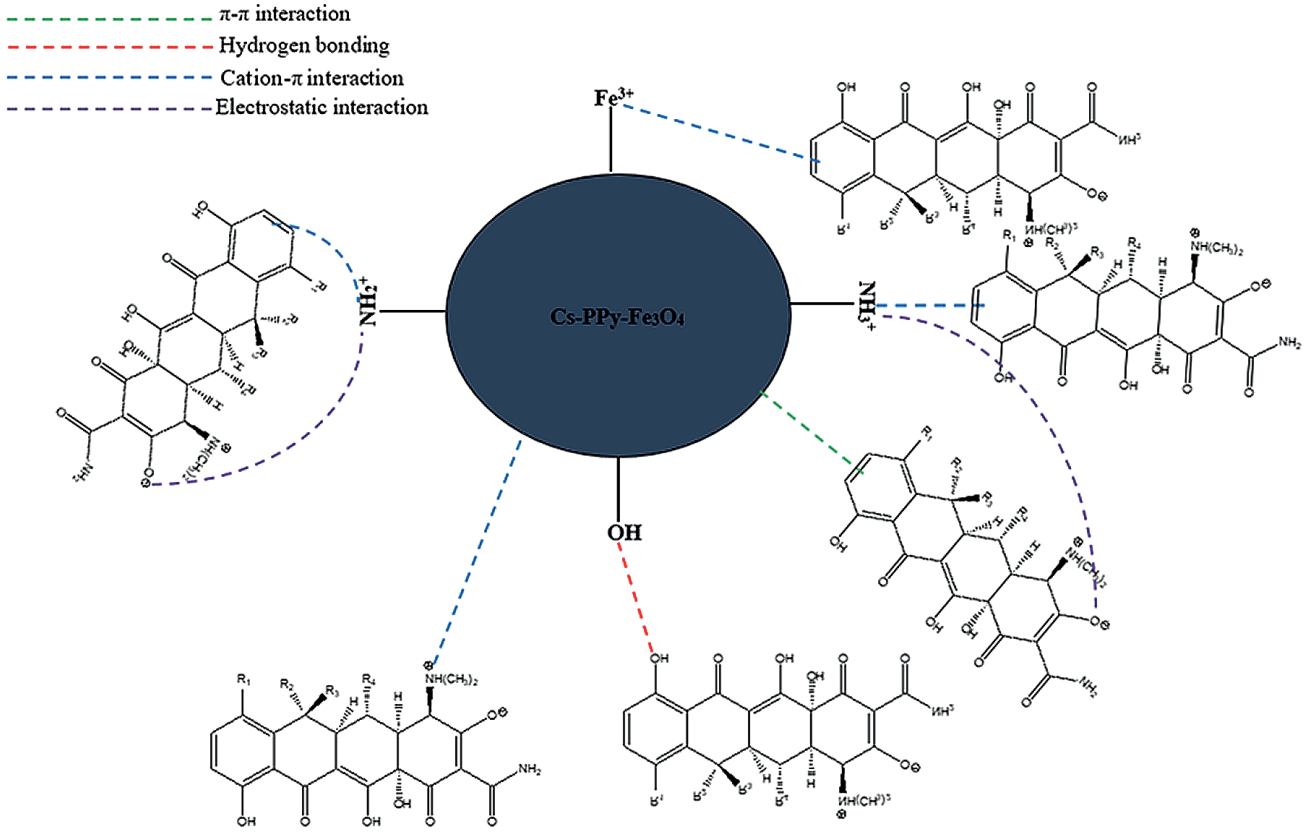

Figure 9. Possible adsorption mechanism of TCs onto Cs-PPy-Fe_3O_4 composite

Table 7. Removal of TCs from wastewater samples (n = 2).

	Influent			Effluent		
Tetracyclines	Before removal (mg L-1)	After removal (mg L-1)	% RE	Before removal (mg L-1)	After removal (mg L-1)	% RE
Oxytetracycline	0	-		0	-	
	2.12	0.12	94.2	2.00	0.08	96.1
	4.00	0.20	95.0	3.98	0.11	97.2
	6.04	0.27	95.5	6.12	0.09	98.5
Tetracycline	0	-	-	0	-	
	1.98	0.16	92.1	2.36	0.12	94.8
	4.13	0.25	93.9	4.05	0.18	95.5
	5.22	0.27	94.8	6.00	0.15	97.5
Chlortetracycline	0	-	-	0	-	
	2.03	0.23	88.7	1.99	0.19	90.6
	4.10	0.44	89.4	4.08	0.27	93.3
	6.05	2.13	64.8	6.03	0.34	94.3
Doxycycline	0	-	-	0	-	
	2.01	0.20	90.2	2.33	0.17	92.6
	4.14	0.32	92.2	4.21	0.24	94.3
	6.01	0.36	94.0	5.99	0.21	96.4

REFERENCES

1. Bigas H, Morris T, Sandford B, Adeel Z. The global water crisis: Addressing an urgent security issue. Hamilton: The United Nations University – Institute for Water, Environment and Health; 2012.
2. World Health Organisation. Drinking-water; 2019. https://www.who.int/news-room/fact-sheets/detail/drinking-water (accessed 25 February 2020).
3. Grossi G, Goglio P, Vitali A, Williams A. Livestock and climate change: impact of livestock on climate change and mitigation strategies. Anim Front. 2019;9(1):69–76. https://doi.org/10.1093/af/vfy034.
4. OECD. 2008. Oecd environmental outlook to 2030. Paris.
5. Verlicchi P, Grillini V. Surface water and groundwater quality in south africa and mozambique—analysis of the most critical pollutants for drinking purposes and challenges in water treatment selection. Water. 2020;12(1):305. https://doi.org/10.3390/w12010305.
6. Yang X, Yang C, Yan X. Zeolite imidazolate framework-8 as sorbent for on-line solid-phase extraction coupled with high-performance liquid chromatography for the determination of tetracyclines in water and milk samples. J Chromatogr A. 2013;1304:28–33. https://doi.org/10.1016/j.chroma.2013.06.064.
7. Dai Y, Liu M, Li J, Yang S, Sun Y, Sun Q, Wang W, Lu L, Zhang K, Xu J, et al. A review on pollution situation and treatment methods of tetracycline in groundwater. Sep Sci Technol. 2020;55(5):1005–1021. https://doi.org/10.1080/01496395.2019.1577445.
8. Liu H, Xu G, Li G. Preparation of porous biochar based on pharmaceutical sludge activated by NaOH and its application in the adsorption of tetracycline. J Colloid Interface Sci. 2021;587:271–278. https://doi.org/10.1016/j.jcis.2020.12.014.
9. Jannat Abadi M, Nouri S, Zhiani R, Heydarzadeh H, Motavalizadehkakhky A. Removal of tetracycline from aqueous solution using Fedoped zeolite. Int J Ind Chem. 2019;10(4):291–300. https://doi.org/10.1007/s40090-019-0191-6.
10. Moussavi G, Alahabadi A, Yaghmaeian K, Eskandari M. Preparation, characterisation and adsorption potential of the NH_4Cl-induced activated carbon for the removal of amoxicillin antibiotic from water. Chem Eng J. 2013;217:119–128. https://doi.org/10.1016/j.cej.2012.11.069.
11. Ncibi M, Sillanpää M. Optimised removal of antibiotic drugs from aqueous solutions using single, double and multi-walled carbon nanotubes. J Hazard Mater. 2015;298:102–110. https://doi.org/10.1016/j.jhazmat.2015.05.025.
12. Genç N, Can Dogan E, Yurtsever M. Bentonite for ciprofloxacin removal from aqueous solution. Water Sci Technol. 2013;68(4):848–855. https://doi.org/10.2166/wst.2013.313.
13. Gadipelly C, Marathe K, Rathod V. Effective adsorption of ciprofloxacin hydrochloride from aqueous solutions using metal-organic framework. Sep Sci Technol. 2018;53(17):2826–2832. https://doi.org/10.1080/01496395.2018.1474225.
14. Wu N, Luo Z, Ge Y, Guo P, Du K, Tang W, Du W, Zeng A, Chang C, Fu Q. A novel surface molecularly imprinted polymer as the solid-phase extraction adsorbent for the selective determination of ampicillin sodium in milk and blood samples. J Pharm Anal. 2016;6(3):157–164. https://doi.org/10.1016/j.jpha.2016.01.004.
15. Saleem J, Shahid U, Hijab M, Mackey H, McKay G. Production and applications of activated carbons as adsorbents from olive stones. Biomass Convers Biorefin. 2019;9(4):775–802. https://doi.org/10.1007/s13399-019-00473-7.
16. Yi Z, Tang Q, Jiang T, Cheng Y. Adsorption performance of hydrophobic/hydrophilic silica aerogel for low concentration organic pollutant in aqueous solution. Nanotechnol Rev. 2019;8(1):266–274. https://doi.org/10.1515/ntrev-2019-0025.
17. Liang H, Zhu C, Ji S, Kannan P, Chen F. Magnetic Fe_2O_3/biochar composite prepared in a molten salt medium for antibiotic removal in water. Biochar. 2022;4(1):1–13. https://doi.org/10.1007/s42773-021-00130-1.
18. Li Y, Wang L, Chai F, Jing H, Gao Z, Zhang Q, Zhao X. Highly effective removal of antibiotics from aqueous solution by magnetic $ZnFe_2O_4$/activated carbon composite. Water Sci Technol. 2020;82(5):877–886. https://doi.org/10.2166/wst.2020.389.
19. Ion S, Pavel O, Guzo N, Tudorache M, Coman S, Parvulescu V, Cojocaru B, Jacobsen E. Photocatalytically active supramolecular organic-inorganic magnetic composites as efficient route to remove β-lactam antibiotics from water. Catalysts. 2022;12(9):1044–1055. https://doi.org/10.3390/catal12091044.
20. Li X, Yin Z, Zhai Y, Kang W, Shi H, Li Z. Magnetic solid-phase extraction of four β-lactams using polypyrrole-coated magnetic nanoparticles from water samples by micellar electrokinetic capillary chromatography analysis. J Chromatogr A. 2020;1610:460541. https://doi.org/10.1016/j.chroma.2019.460541.
21. Umer A, Liaqat F, Mahmood A. MoO_3 nanobelts embedded polypyrrole/SIS copolymer blends for improved electro-mechanical dual applications. Polymers (Basel). 2020;12(2):353–365. https://doi.org/10.3390/polym12020353.

22. Chen Y, Feng H, Li L, Shang S, Chun-Wah Yuen M. Synthesis and properties of polypyrrole/chitosan composite hydrogels. J Macromol Sci Part A Pure Appl Chem. 2013;50(12):1225–1229. https://doi.org/10.1080/10601325.2013.843403.
23. Ansari R, Mosayebzadeh Z. Removal of basic dye methylene blue from aqueous solutions using sawdust and sawdust coated with polypyrrole. J Iran Chem Soc. 2010;7(2):339–350. https://doi.org/10.1007/BF03246019.
24. Leonel A, Mansur A, Mansur H. Advanced functional nanostructures based on magnetic iron oxide nanomaterials for water remediation: A review. Water Res. 2021;190:116693. https://doi.org/10.1016/j.watres.2020.116693.
25. Nezhadali A, Koushali S, Divsar F. Synthesis of polypyrrole – chitosan magnetic nanocomposite for the removal of carbamazepine from wastewater: adsorption isotherm and kinetic study. J Environ Chem Eng. 2021;9(4):105648. https://doi.org/10.1016/j.jece.2021.105648.
26. Reis E, Gorza F, Pedro G, Maciel B, daSilva R, Ratkovski G, de Melo C. (Maghemite/chitosan/polypyrrole) nanocomposites for the efficient removal of Cr (VI) from aqueous media. J Environ Chem Eng. 2021;9(1):104893. https://doi.org/10.1016/j.jece.2020.104893.
27. Bagheri H, Roostaie A, Baktash M. A chitosan–polypyrrole magnetic nanocomposite as u-sorbent for isolation of naproxen. Anal Chim Acta. 2014;816:1–7. https://doi.org/10.1016/j.aca.2014.01.028.
28. Liao Q, Hu L, Luo L. A chitosan–polypyrrole@Fe_3O_4 nanocomposite for magnetic solid-phase extraction of macrolides from swine urine samples. Anal Methods. 2015;7(6):2806–2812. https://doi.org/10.1039/C4AY02907K.
29. Shalaby AR, Salama NA, Abou-Raya SH, Emam WH, Mehaya FM. Validation of HPLC method for determination of tetracycline residues in chicken meat and liver. Food Chem. 2011;124(4):1660–1666. https://doi.org/10.1016/j.foodchem.2010.07.048.
30. Ahamad T, Naushad M, Al-shahrani T, Al-hokbany N, Alshehri S. Preparation of chitosan based magnetic nanocomposite for tetracycline adsorption: kinetic and thermodynamic studies. Int J Biol Macromol. 2020;147:258–267. https://doi.org/10.1016/j.ijbiomac.2020.01.025.
31. Rathod M, Haldar S, Basha S. Nanocrystalline cellulose for removal of tetracycline hydrochloride from water via biosorption: Equilibrium, kinetic and thermodynamic studies. Ecol Eng. 2015;84:240–249. https://doi.org/10.1016/j.ecoleng.2015.09.031.
32. Usman M, Ibrahim N, Shameli K, Zainuddin N, Yunus W. Copper nanoparticles mediated by chitosan: synthesis and characterisation via chemical methods. Molecules. 2012;17(12):14928–14936. https://doi.org/10.3390/molecules171214928.
33. Sharma G, Jeevanandam P. A facile synthesis of multifunctional iron oxide@Ag core–shell nanoparticles and their catalytic applications. Eur J Inorg Chem. 2013;2013(36):6126–6136. https://doi.org/10.1002/ejic.201301193.
34. Jose B, Thomas F. Photocatalytic degradation of methylene blue using iron oxide nanoparticles synthesised using annona muricata leaf extract. Int J Pharm Pharm Sci. 2020;12:46–51. https://doi.org/10.22159/ijpps.2020v12i10.38821.
35. Ramesan M, Santhi V. Synthesis, characterisation, conductivity and sensor application study of polypyrrole/silver doped nickel oxide nanocomposites. Compos Interfaces. 2018;25(8):725–741. https://doi.org/10.1080/09276440.2018.1439626.
36. López-García F, Canché-Escamilla G, Ocampo-Flores A, Roquero-Tejeda P, Ordóñez L. Controlled size nano-polypyrrole synthetised in micro-emulsions as Pt support for the ethanol electro-oxidation reaction. Int J Electrochem Sci. 2013;8(3):3794–3813. https://doi.org/10.1016/S1452-3981(23)14432-4.
37. Tikish T, Kumar A, Kim J. Electrical and optical properties of polypyrrole and polyaniline blends. Polym Sci Ser A. 2020;62(6):680–690. https://doi.org/10.1134/S0965545X20330056.
38. Gibot P, Goetz V. Polypyrrole material for the electrostatic discharge sensitivity mitigation of Al/SnO_2 energetic composites. J Appl Polym Sci. 2021;138(29):50752. https://doi.org/10.1002/app.50752.
39. Fu Y, Su Y, Manthiram A. Sulfur-polypyrrole composite cathodes for lithium-sulfur batteries. J Electrochem Soc. 2012;159(9):A1420–A1424. https://doi.org/10.1149/2.027209jes.
40. Suárez-Guevara J, Ayyad O, Gómez-Romero P. Copper@polypyrrole nanocables. Nanoscale Res Lett. 2012;7(1):521–526. https://doi.org/10.1186/1556-276X-7-521.
41. Chouli Y, Belkhadem-Mokhtari F, Abou-Zeid S, Dragoe D, Saint-Martin R, Brisset F, Remita H, Remita S. Superior photocatalytic activity of polypyrrole nanostructures prepared by radiolysis in water and dichloromethane. Radiat Phys Chem. 2022;195:110079. https://doi.org/10.1016/j.radphyschem.2022.110079.
42. Dhillon A, Kaur A, Srivastava A, Avasthi D. Experimental investigations of semi-crystalline plasma polymerised polypyrrole for surface coating. Prog Org Coat. 2010;69(4):396–401. https://doi.org/10.1016/j.porgcoat.2010.08.002.
43. Aziz S, Karim W, Brza M, Abdulwahid R, Saeed S, Al-Zangana S, Kadir M. Ion transport study in CS: POZ based polymer membrane electrolytes using trukhan model. Int J Mol Sci. 2019;20(21):5265. https://doi.org/10.3390/ijms20215265.
44. Aziz SB, Marf AS, Dannoun EMA, Brza MA, Abdullah RM. The study of the degree of crystallinity, electrical equivalent circuit, and dielectric properties of polyvinyl alcohol (PVA)-based biopolymer electrolytes. Polymers (Basel). 2020;12:2184. https://doi.org/10.3390/polym12102184.
45. Namvari M, Namazi H. Clicking graphene oxide and Fe_3O_4 nanoparticles together: an efficient adsorbent to remove dyes from aqueous solutions. Int J Environ Sci Technol. 2014;11(6):1527–1536. https://doi.org/10.1007/s13762-014-0595-y.
46. Swanson H, McMurdie H, Morris M, Evans E. Standard x-ray diffraction powder patterns. In: Commerce UDo, editor. Washington DC: US Department of Commerce; 1967, 100 p. https://doi.org/10.6028/NBS.MONO.25-5.
47. Gaur S, Ghosh A, Singh V, editors. Influence of nickel oxide nanoparticle on the structural, electrical and dielectric properties of polypyrrole nanocomposite. International Conference on Advances in Basic Science. Bahal: AIP Publishing; 2019.
48. Periakaruppan R, Chen X, Thangaraj K, Jeyaraj A, Nguyen H, Yu Y, Hu S, Lu L, Li X. Utilization of tea resources with the production of superparamagnetic biogenic iron oxide nanoparticles and an assessment of their antioxidant activities. J Clean Prod. 2021;278:123962. https://doi.org/10.1016/j.jclepro.2020.123962.
49. Cabrera L, Gutierrez S, Morales M, Menendez N, Herrasti P. Magnetic conducting composites based on polypyrrol and iron oxide nanoparticles synthesised via electrochemistry. J Magn Magn Mater. 2009;321(14):2115–2120. https://doi.org/10.1016/j.jmmm.2009.01.021.
50. Levine K, Tallman D, Bierwagen G. The mediated electrodeposition of polypyrrole on aluminium alloy. Aust J Chem. 2005;58(4):294–301. https://doi.org/10.1071/CH04289.
51. Bashir T, Shakoor A, Ahmed E, Niaz N, Akhtar M, Raza M, Malik M, Foot P. Polypyrrole-Fe_2O_3 nanocomposites with high dielectric constant: in situ chemical polymerisation. Polym Polymer Compos. 2018;26(3):233–241. https://doi.org/10.1177/096739111802600303.
52. Hsu L, Liu Y, Syu C, Huang M, Tzou Y, Teah H. Adsorption of tetracycline on Fe (hydr)oxides: effects of pH and metal cation (Cu^{2+},$Zn^{2+}$and Al^{3+}) addition in various molar ratios. R Soc Open Sci. 2018;5(3):171941. https://doi.org/10.1098/rsos.171941.
53. Chico J, vanHolthoon F, Zuidema T. Ion suppression study for tetracyclines in feed. Chromatogr Res Int. 2012;2012:135854. https://doi.org/10.1155/2012/135854.
54. Gopal G, Alex S, Chandrasekaran N, Mukherjee A. A review on tetracycline removal from aqueous systems by advanced treatment techniques. RSC Adv. 2020;10(45):27081–27095. https://doi.org/10.1039/D0RA04264A.
55. Diephuis WR, Molloy AL, Boltz LL, Porter TB, Aragon Orozco A, Duron R, Crespo D, George LJ, Reiffer AD, Escalera G, et al. The effect of agglomeration on arsenic adsorption using iron oxide nanoparticles. Nanomaterials (Basel). 2022;12(9):1598. https://doi.org/10.3390/nano12091598.
56. Alidadi H, Dolatabadi M, Davoudi M, Barjasteh-Askari F, Jamali-Behnam F, Hosseinzadeh A. Enhanced removal of tetracycline using modified sawdust: Optimisation, isotherm, kinetics, and regeneration studies. Process Saf Environ Prot. 2018;117:51–60. https://doi.org/10.1016/j.psep.2018.04.007.
57. Aslan S, Şirazi M. Adsorption of sulfonamide antibiotic onto activated carbon prepared from an agro-industrial by-product as low-cost adsorbent: Equilibrium, thermodynamic, and kinetic studies. Water Air Soil Pollut. 2020;231(5):222–241. https://doi.org/10.1007/s11270-020-04576-0.
58. Ragab AH, Hussein HS, Ahmed IS, Abualnaja KM, AlMasoud N. An efficient strategy for enhancing the adsorption of antibiotics and drugs from

aqueous solutions using an effective limestone-activated carbon–alginate nanocomposite. Molecules. 2021;26(17):5180. https://doi.org/10.3390/molecules26175180.

59. Chen X. Modeling of experimental adsorption isotherm data. Information (Basel). 2015;6(1):14–22. https://doi.org/10.3390/info6010014.
60. Hu Q, Zhang Z. Application of Dubinin–Radushkevich isotherm model at the solid/solution interface: A theoretical analysis. J Mol Liq. 2019;277:646–648. https://doi.org/10.1016/j.molliq.2019.01.005.
61. Rajahmundry G, Garlapati C, Kumar P, Alwi R, Vo D. Statistical analysis of adsorption isotherm models and its appropriate selection. Chemosphere. 2021;276:130176. https://doi.org/10.1016/j.chemosphere.2021.130176.
62. Rahman M, Pal A, Uddin K, Thu K, Saha B. Statistical analysis of optimised isotherm model for maxsorb III/ethanol and silica gel/water pairs. Evergreen. 2018;5(4):1–12. https://doi.org/10.5109/2174852.
63. Sreńscek-Nazzal J, Narkiewicz U, Morawski A, Wróbel R, Michalkiewicz B. Comparison of optimised isotherm models and error functions for carbon dioxide adsorption on activated carbon. J Chem Eng Data. 2015;60(11):3148–3158. https://doi.org/10.1021/acs.jced.5b00294.
64. Álvarez-Torrellas S, Ribeiro R, Gomes H, Ovejero G, García J. Removal of antibiotic compounds by adsorption using glycerol-based carbon materials. Chem Eng J. 2016;296:277–288. https://doi.org/10.1016/j.cej.2016.03.112.
65. Madikizela L, Zunngu S, Mlunguza N, Tavengwa N, Mdluli P, Chimuka L. Application of molecularly imprinted polymer designed for the selective extraction of ketoprofen from wastewater. Water SA. 2018;44(3 July):406–418. https://doi.org/10.4314/wsa.v44i3.08.
66. Dehghan A, Dehghani M, Nabizadeh R, Ramezanian N, Alimohammadi M, Najafpoor A. Adsorption and visible-light photocatalytic degradation of tetracycline hydrochloride from aqueous solutions using 3D hierarchical mesoporous BiOI: synthesis and characterisation, process optimisation, adsorption and degradation modeling. Chem Eng Res Des. 2018;129:217–230. https://doi.org/10.1016/j.cherd.2017.11.003.
67. Azhar M, Abid H, Sun H, Periasamy V, Tadé M, Wang S. *E*xcellent performance of copper based metal organic framework in adsorptive removal of toxic sulfonamide antibiotics from wastewater. J Colloid Interface Sci. 2016;478:344–352. https://doi.org/10.1016/j.jcis.2016.06.032.
68. Korkut F, Saloglu D. Synthesis, characterisation, and tetracycline adsorption behavior of activated carbon dopped alginate beads: Isotherms, kinetics, thermodynamic, and adsorption mechanism. Desalination Water Treat. 2020;206:315–330. https://doi.org/10.5004/dwt.2020.26305.
69. Cáceres L, Escudey M, Fuentes E, Báez M. Modeling the sorption kinetic of metsulfuron-methyl on andisols and ultisols volcanic ash-derived soils: kinetics parameters and solute transport mechanisms. J Hazard Mater. 2010;179(1-3):795–803. https://doi.org/10.1016/j.jhazmat.2010.03.074.
70. Hidayat A, Sulistiono D, Murwani I, Endrawati B, Fansuri H, Zulfa L, Ediati R. Linear and nonlinear isotherm, kinetic and thermodynamic behavior of methyl orange adsorption using modulated Al_2O_3@UiO-66 via acetic acid. J Environ Chem Eng. 2021;9(6):106675. https://doi.org/10.1016/j.jece.2021.106675.
71. Pholosi A, Naidoo E, Ofomaja A. Intraparticle diffusion of Cr(VI) through biomass and magnetite coated biomass: A comparative kinetic and diffusion study. S Afr J Chem Eng. 2020;32:39–55. https://doi.org/10.1016/j.sajce.2020.01.005.
72. Luo B, Huang G, Yao Y, An C, Li W, Zheng R, Zhao K. Comprehensive evaluation of adsorption performances of carbonaceous materials for sulfonamide antibiotics removal. Environ Sci Pollut Res Int. 2021;28(2):2400–2414. https://doi.org/10.1007/s11356-020-10612-7.
73. LópezLuna J, RamírezMontes L, MartinezVargas S, Martínez A, MijangosRicardez O, GonzálezChávez M, CarrilloGonzález R, SolísDomínguez F, CuevasDíaz M, VázquezHipólito V. Linear and nonlinear kinetic and isotherm adsorption models for arsenic removal by manganese ferrite nanoparticles. SN Appl Sci. 2019;1(8):950–969. https://doi.org/10.1007/s42452-019-0977-3.
74. Qhubu M, Nomngongo P, Pakade V. Exploring the iron oxide functionalised biobased carbon-silica-polyethyleneimine composites for hexavalent chromium removal from dilute aqueous solutions. Water. 2021;13(21):3081. https://doi.org/10.3390/w13213081.
75. Wang J, Liu X, Yang M, Han H, Zhang S, Ouyang G, Han R. Removal of tetracycline using modified wheat straw from solution in batch and column modes. J Mol Liq. 2021;338:116698. https://doi.org/10.1016/j.molliq.2021.116698.
76. Lin Y, Xu S, Li J. Fast and highly efficient tetracyclines removal from environmental waters by graphene oxide functionalised magnetic particles. Chem Eng J. 2013;225:679–685. https://doi.org/10.1016/j.cej.2013.03.104.
77. Zeng G, Liu Y, Ma X, Fan Y. Fabrication of magnetic multi-template molecularly imprinted polymer composite for the selective and efficient removal of tetracyclines from water. Front Environ Sci Eng. 2021;15(5):107–118. https://doi.org/10.1007/s11783-021-1395-5.
78. Zaidi S, Sivasankar V, Chaabane T, Alonzo V, Omine K, Maachi R, Darchen A, Prabhakaran M. Separate and simultaneous removal of doxycycline and oxytetracycline antibiotics by electro-generated adsorbents (EGAs). J Environ Chem Eng. 2019;7(1):102876. https://doi.org/10.1016/j.jece.2018.102876.
79. Hubetska T, Kobylinska N, García J. Efficient adsorption of pharmaceutical drugs from aqueous solution using a mesoporous activated carbon. Adsorption. 2020;26(2):251–266. https://doi.org/10.1007/s10450-019-00143-0.
80. Wang H, Lou X, Hu Q, Sun T. Adsorption of antibiotics from water by using chinese herbal medicine residues derived biochar: preparation and properties studies. J Mol Liq. 2021;325:114967. https://doi.org/10.1016/j.molliq.2020.114967.